JAMES | Journal of Advances in Modeling Earth Systems

RESEARCH ARTICLE
10.1029/2018MS001554

Eddy Influences on the Hadley Circulation

Nicholas A. Davis[1,2,3,4] **and Thomas Birner**[1,5]

[1]Department of Atmospheric Science, Colorado State University, Fort Collins, CO, USA, [2]Now at Atmospheric Chemistry Observations and Modeling Division, National Center for Atmospheric Research, Boulder, CO, USA, [3]Cooperative Institute for Research in Environmental Sciences, University of Colorado Boulder, Boulder, CO, USA, [4]Chemical Sciences Division, NOAA Earth System Research Laboratory, Boulder, CO, USA, [5]Now at Meteorological Institute Munich, Ludwig Maximilians University, Munich, Germany

Key Points:
- New idealized modeling technique separates time-mean eddy and mean flow components
- Eddies fundamentally alter Hadley cell structure and momentum transport
- Previous studies may have underestimated the impact of eddies on the mean meridional circulation

Correspondence to:
N. A. Davis,
nadavis@ucar.edu

Citation:
Davis, N. A., & Birner, T. (2019). Eddy influences on the Hadley circulation. *Journal of Advances in Modeling Earth Systems*, *11*, 1563–1581. https://doi.org/10.1029/2018MS001554

Received 5 NOV 2018
Accepted 19 APR 2019
Accepted article online 25 APR 2019
Published online 7 JUN 2019

Abstract Variations in the width and strength of the Hadley cells are associated with many radiative, thermodynamic, and dynamical forcings. The physical mechanisms driving these responses remain unclear, in part because of the interactive nature of eddy-mean flow adjustment. Here, a modeling framework is developed which separates the mean flow and time-mean eddy flow in a gray radiation general circulation model with simple representations of ocean heat transport and ozone. In the absence of eddies, with moist convection and weak numerical damping, the Hadley cell is confined to the upper troposphere and has a vanishingly small poleward momentum flux. Eddies allow the cell to extend down to the surface, double its heat transport, and flux momentum poleward, the latter two being basic consequences of a deepening of the circulation. Because of convection and damping—which mimics, in part, the effect of eddy stresses—previous work may have underestimated the impact of eddies on earth's circulation. Quasigeostrophic eddy fluxes are sufficient to produce Hadley and Ferrel cells, but with a substantially greater Hadley cell strength than when all eddy impacts are considered, including eddy fluxes of moisture, mass, and momentum and eddy impacts on surface fluxes and clouds.

1. Introduction

Model experiments indicate that a poleward expansion of the Hadley cells is a fundamental response of the climate system to greenhouse gas forcings (Davis et al., 2016; Grise & Polvani, 2016; Hu et al., 2013; Lu et al., 2007). Because of the sharp gradients in temperature, precipitation, and humidity at the cells' edges, a poleward expansion of the circulation has the potential to project strongly onto surface climate (Birner et al., 2014; Seidel et al., 2008). Understanding Hadley cell expansion is therefore crucial for understanding the future impacts of anthropogenic and natural climate changes. But a more basic question is what sets the width and strength of the Hadley circulation in the mean? Unraveling this answer can only better inform our understanding of future changes.

Axisymmetric models and scaling theories are the limit of an eddy-free Hadley circulation, an ideal starting point for assessing the role of eddies in its climatology and response to forcings (Fang & Tung, 1999; Held, 2000; Held & Hou, 1980; Lindzen & Hou, 1988; Walker & Schneider, 2005). Eddies drive some fraction of the meridional circulation, influencing its strength and width over a wide range of climates (Caballero, 2007; Ceppi & Hartmann, 2013; Frierson, Lu, et al., 2007; Walker & Schneider, 2006; Zurita-Gotor & Álvarez-Zapatero, 2018). In both dry and moist atmospheres, the Hadley cell edge is highly correlated with the latitude at which eddies deepen and reach the upper troposphere (Korty & Schneider, 2008; Levine & Schneider, 2015). There, Rossby waves transition from upward propagation and growth to meridional propagation and dissipation, with first order impacts on the zonal momentum balance. However, this latitude can be influenced by the upper tropospheric zonal winds associated with the Hadley circulation itself (Bordoni & Schneider, 2010; Schneider & Bordoni, 2008; Sobel & Schneider, 2009; Zurita-Gotor & Álvarez-Zapatero, 2018). It is difficult to understand the impact of the eddies on the mean flow through a budget analysis because of this wave-mean flow feedback (Becker et al., 1997; Kim & Lee, 2001). Moisture may influence how the eddies shape the circulation, as latent heating is an important diabatic process in both the Hadley circulation and the midlatitude storm tracks (Pauluis et al., 2008).

Becker et al. (1997) and Kim and Lee (2001) examine simulations of axisymmetric and eddy-permitting atmospheres, finding that eddies generally strengthen the Hadley cells. However, both represent convective

heating as a steady-state, noninteractive forcing in their respective models, and as in Held and Hou (1980) and other studies relax temperatures to an equilibrium state. As the response of the mean flow to eddies depends on convective heating properties and radiative timescales (Becker et al., 1997; Kim & Lee, 2001), it remains to be seen how eddies impact the circulation in a model with more interactive representations of convection, radiation, and moisture. Another fundamental question is how the use of damping in these axisymmetric models does or does not impact the interpretation of the role of eddies in driving the circulation. As an example, viscosity—which relates the flow shear to the stress—and eddy stresses both disrupt angular momentum conservation to the degree that viscosity can reasonably approximate the impact of eddy stresses (Adam & Paldor, 2010; Walker & Schneider, 2005).

This study revisits the topic of the influence of eddies on the mean state of the Hadley circulation with the dual goals of further understanding the fundamental differences between axisymmetric and eddy-permitting circulations and, in future work, separating the eddy and mean flow responses to radiative forcings. We develop a new modeling framework within a gray radiation aquaplanet model (GRAM) whereby the global circulation is decomposed into mean flow and (time-mean) eddy forcings, allowing us to selectively add and subtract eddy forcings of different variables and of varying dynamical scalings. In these simulations, the model implicitly solves for the zonal-mean components of the flow alone.

In section 2 we describe the reanalysis data used to assess the model, the model formulation, and the model's climatology. Section 3 describes the method used to separate the eddy and mean parts of the flow. In section 4 we use the vertically integrated momentum and heat budgets to demonstrate that eddies fundamentally alter the behavior of the Hadley cells. We conclude with a discussion of these results and their implications in sections 5 and 6.

2. Model and Data

We use monthly mean ozone, temperature, and horizontal winds from the Modern Era Retrospective Reanalysis 2 (MERRA2) reanalysis to assess the climate of GRAM (Gelaro et al., 2017). In all cases we use the instantaneous fields, and we use the assimilation rather than analysis product.

This study uses the GRAM based on the Geophysical Fluid Dynamics Laboratory dynamical core and described in Frierson et al. (2006). Unless otherwise noted, we use the same parameter values as in Frierson et al. (2006). Unlike a dynamical core in a Held-Suarez configuration, GRAM includes an idealized radiation scheme based on the two-stream plane-parallel approximation, with upward and downward shortwave and longwave radiative fluxes. Absorption of longwave radiation is determined through a fixed optical depth field, defined as

$$\tau_{LW}(p,\phi) = \tau_0(\phi)\left\{ s\left(\frac{p}{p_0}\right) + (1-s)\left(\frac{p}{p_0}\right)^4 \right\} \tag{1}$$

where p is the pressure, ϕ is the latitude, $0 \leq s \leq 1$ determines the linearity of the optical depth field in the stratosphere (here taken to be 0.1), p_0 is the reference surface pressure of 1,000 hPa, and $\tau_0(\phi)$ is a latitude-dependent surface optical depth given by

$$\tau_0(\phi) = \tau_{0,e} + (\tau_{0,p} - \tau_{0,eq})\sin^2(\phi) \tag{2}$$

where $\tau_{0,e}$ and $\tau_{0,p}$ are the equatorial and polar surface optical depths. The longwave optical depth decreases toward the poles, reflecting the meridional profile of water vapor pressure, and decreases upward, reflecting the integrated mass from a given level to the top of the atmosphere. Insolation is prescribed as in Frierson et al. (2006) and reflects the annual mean with nonzero insolation at the poles rather than equinox conditions.

Unaltered, the gray radiation scheme produces some unrealistic features in the zonal circulation, with a single merged jet instead of distinguishable eddy-driven, subtropical, and stratospheric jets (Figure 1b). To make the stratosphere more comparable to Earth's, we apply a shortwave optical depth to mimic the radiative effects of ozone. In Earth's climate, the concentration of ozone peaks at approximately 80 hPa at the poles with a 65-hPa half-width and at approximately 30 hPa at the equator with a 20-hPa half-width, with the total column ozone peaking at the poles (Figure 2). To approximate this ozone distribution, the shortwave optical depth is prescribed here as

$$\tau_s(p) = \frac{\tau_{0,s}\sqrt{\pi}}{2}\left\{ \frac{\cos^2(0.3\phi)}{3}\left[\mathrm{erf}\left(\frac{p-p_{\mathrm{center}}}{p_{\mathrm{width}}}\right)+1\right] + \frac{1}{4}\left[\mathrm{erf}\left(\frac{p-140}{60}\right)+1\right]\right\} \tag{3}$$

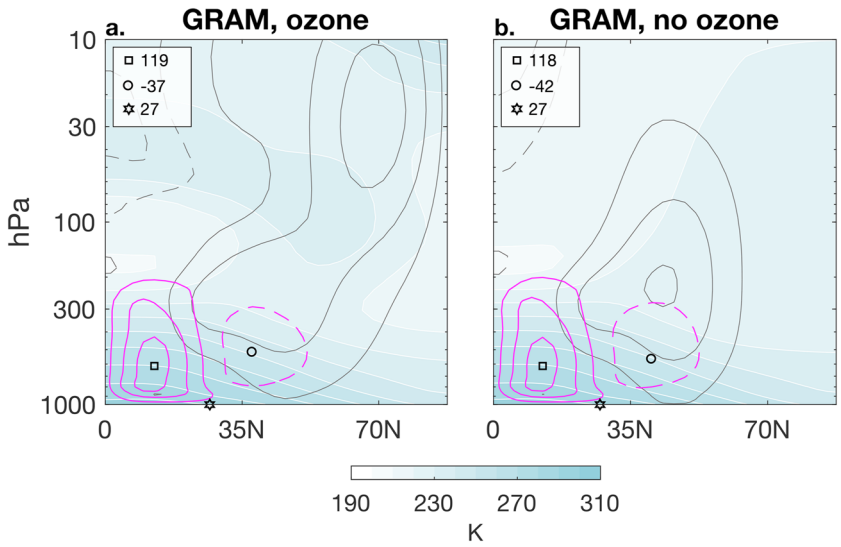

Figure 1. Zonal-mean climate of GRAM (a) with and (b) without an idealized ozone distribution. (shading) Temperature every 10 K, (black contours) zonal-mean zonal wind every 10 m/s, and (magenta contours) mean meridional stream function every 40 $\times 10^9$ kg/s starting from 20 $\times 10^9$ kg/s. Negative zonal-mean zonal wind and mean meridional stream function indicated by dashed contours. The location and value of the stream function maximum and minimum are indicated by the square and circle, respectively, and the edge of the Hadley circulation in degrees latitude is indicated by the star. GRAM = gray radiation aquaplanet model.

where $\tau_{0,s} = 0.008$ is the surface shortwave optical depth at the equator (and also the approximate fraction of insolation absorbed by the atmosphere), and p_{center} and p_{width} are the central pressure and half-width of the tropical psuedo-ozone distribution, defined as

$$p_{center} = 130 - 90\cos^2(0.9\phi) \tag{4}$$

$$p_{width} = 20 + 40\sin^2(\phi) \tag{5}$$

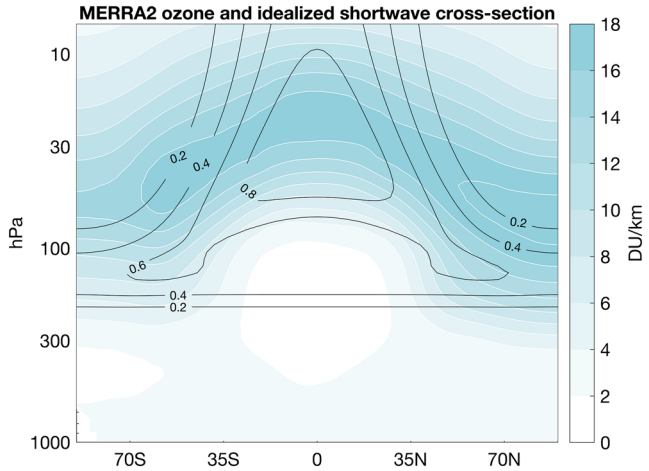

Figure 2. (shading) Ozone distribution in Dobson units per kilometer from MERRA2 and (black contours) idealized shortwave psuedo mixing ratio in gray radiation aquaplanet model. Psuedo mixing ratio in arbitrary units scaled to a maximum value of 1—see text for details. MERRA2 = Modern Era Retrospective Reanalysis 2.

The two terms in equation (3) model the ozone distribution above and below 200 hPa, respectively. The vertical derivative of the ozone optical depth is displayed in Figure 2, scaled to an arbitrary value of 1, along with the annual-mean ozone from MERRA2 in Dobson units per kilometer. For a gas with a constant absorption coefficient, the vertical derivative of the optical depth is equivalent by a factor to the mixing ratio of the gas. Our ozone distribution is not meant to perfectly mimic Earth's, but instead to produce a more realistic stratosphere in GRAM (Figure 1a). The troposphere in GRAM is nearly 100 hPa shallower than Earth's; hence, we extend the ozone field downward to accommodate the model's unique climatology. Changes to the prescribed shortwave optical depth would need to be considered for other iterations of this model with different climatologies.

Water vapor is modeled as an active tracer with a finite volume parabolic advection scheme. Large-scale condensation occurs should a grid box reach supersaturation, and the ice phase is neglected. Precipitation and reevaporation of falling precipitate is instantaneous. To produce surface precipitation, then, the column must be saturated from the surface up to the precipitating level. In addition to resolved condensation, the model runs a simplified Betts-Miller convection scheme with both shallow and deep modes. A full description of the scheme can be found in Frierson (2007). To summarize, the scheme adjusts temperature and specific

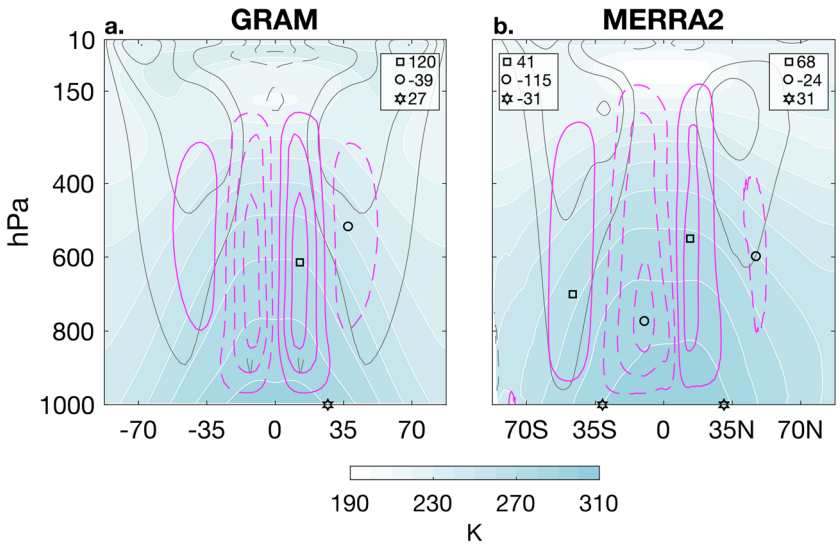

Figure 3. As in Figure 1 but for (a) GRAM and (b) MERRA2 during March-April-May-September-October-November. GRAM = gray radiation aquaplanet model; MERRA2 = Modern Era Retrospective Reanalysis 2.

humidity to reference profiles. Deep convection occurs if the convective available potential energy is greater than the convective inhibition and there is more moisture in the column than there is in the reference profile. Shallow convection occurs if only the former is satisfied, and the resulting adjustment produces no net precipitation. We run the model with an adjustment timescale of 6 hr and a fixed psuedoadiabat relative humidity of 80%. The scheme does not diffuse momentum.

Surface fluxes of heat, moisture, and momentum are modeled with bulk formulas, with drag and vertical diffusion coefficients calculated via a simplified Monin-Obukhov similarity theory. Vertical diffusion occurs within the boundary layer and vanishes at the boundary layer top, which is set by the critical Richardson number. The ocean surface is a mixed layer with a fixed heat capacity of 1×10^7 J$\cdot^{-1}\cdot$m^{-2}, equivalent to a mixed layer depth of approximately 2.3 m. At this depth, the ocean and atmosphere have approximately the same total heat capacity.

Without ocean heat transport, the model produces a Hadley cell stream function maximum of 180×10^9 kg/s, far in excess of the modeled 115×10^9 kg/s in the Southern Hemisphere in MERRA2 (Figure 3; GRAM has no topography, and as the Southern Hemisphere has less land area than the Northern Hemisphere, it is a reasonable analogue). To make the Hadley cell intensity more representative of Earth's, we parameterize a wind-driven meridional overturning circulation in the mixed layer as in Levine and Schneider (2011), with further detail provided by Klinger and Marotzke (2000). Oceanic meridional heat transport occurs within the equatorial belt of easterlies, with subduction in the subtropics and upwelling at the equator. A Gaussian smoother is applied to diffuse the unrealistically high cooling that occurs along the equator due to the vanishing Coriolis parameter. For simplicity and to ensure stable numerical calculations, the ocean heat flux is assumed to be zonally symmetric and driven by zonal-mean surface winds.

We run the model at T42 spectral resolution with 40 vertical levels, spaced in sigma coordinates as $\sigma = exp[-5(0.05\hat{z} + 0.95\hat{z}^3)]$, where $\hat{z}$ are evenly spaced between 0 and 1. This results in approximately 15 levels in the stratosphere and 7 levels in the boundary layer. The numerical scheme uses fourth-order hyperdiffusion and a time step of 600 s with semi-implicit leapfrog time stepping. This time step is substantially shorter than what is required by the Courant-Friedrichs-Lewy condition because the axisymmetric version of the model rapidly generates symmetric instabilities if the time step is not sufficiently short. To run an axisymmetric simulation, the model is merely initialized in a zonally symmetric state. The numerics are otherwise identical between the axisymmetric and eddy-permitting simulations. In contrast to previous work, neither the eddy-permitting nor the axisymmetric simulations have vertical diffusion (except within the boundary layer). A hole filling algorithm is used to ensure water vapor pressure is never negative, and an additive constant ensures mass, water vapor, and energy conservation after each time step. All simulations branch from 2,000 day spin-ups and run for 1,000 days. Only the last 600 days are used in our analysis.

GRAM's zonal-mean climate resembles the Southern Hemisphere equinox climate in MERRA2 (Figure 3). Both have well-defined subtropical, eddy-driven, and polar jets, and the Ferrel cells are of similar intensity. The intensity of the Hadley cell in GRAM is within five percent of the intensity of the Southern Hemisphere Hadley cell and twice as strong as the Northern Hemisphere Hadley cell (Figure 3). Despite a minimal representation of moist convection, radiation, and stratospheric dynamics, GRAM has a cold-point tropopause temperature within 10 K of what is modeled in MERRA2. If the troposphere were deeper in GRAM, one would expect the cold-point tropopause temperature to be even closer to MERRA2. Jucker and Gerber (2017) produce a realistic cold point and tropical tropopause layer in a similar model with simple topography and a more realistic radiation scheme.

3. Separating the Eddy and Mean Flow Components in the Model

Consider the zonal-mean prognostic equations for momentum, heat, mass, and moisture in the eddy-permitting simulations in spherical isobaric coordinates, separated into mean flow and eddy components,

$$\frac{\partial[u]}{\partial t}+\frac{[v]}{a\cos(\phi)}\frac{\partial}{\partial\phi}\left([u]\cos(\phi)\right)+[\omega]\frac{\partial[u]}{\partial p}-f[v]= -\frac{1}{a\cos^2(\phi)}\frac{\partial}{\partial\phi}\left([u'v']\cos^2(\phi)\right)-\frac{\partial[\omega'u']}{\partial p}+[F_\lambda] \tag{6}$$

$$\frac{\partial[v]}{\partial t}+\frac{[v]}{a}\frac{\partial[v]}{\partial\phi}+[\omega]\frac{\partial[v]}{\partial p}+f[u]+\frac{[u]^2\tan(\phi)}{a}+\frac{1}{a}\frac{\partial[\Phi]}{\partial\phi}= -\frac{1}{a\cos(\phi)}\frac{\partial}{\partial\phi}\left([v'^2]\cos(\phi)\right)-\frac{\partial[\omega'v']}{\partial p}-\frac{[u'^2]\tan(\phi)}{a}+[F_\phi] \tag{7}$$

$$\frac{\partial[T]}{\partial t}+\frac{[v]}{a}\frac{\partial[T]}{\partial\phi}+[\omega]\frac{\partial[T]}{\partial p}-\frac{R_d[T][\omega]}{c_p p}= \frac{R_d[\omega'T']}{c_p p}-\frac{1}{a\cos(\phi)}\frac{\partial}{\partial\phi}\left([v'T']\cos(\phi)\right)-\frac{\partial[\omega'T']}{\partial p}+[\dot{T}] \tag{8}$$

$$\frac{\partial[p_s]}{\partial t}=-\int_0^{p_s}\nabla\cdot[\vec{v_H}][p]\mathrm{d}p-\int_0^{p_s}\nabla\cdot[\vec{v_H}'p']\mathrm{d}p \tag{9}$$

$$\frac{\partial[q]}{\partial t}+\frac{[v]}{a}\frac{\partial[q]}{\partial\phi}+[\omega]\frac{\partial[q]}{\partial p}=-\frac{1}{a\cos(\phi)}\frac{\partial}{\partial\phi}\left([v'q']\cos(\phi)\right)-\frac{\partial[\omega'q']}{\partial p}+[\dot{q}] \tag{10}$$

where T is the temperature; u, v, and ω are the zonal, meridional, and vertical winds; $\vec{v_H}$ is the horizontal wind vector; a is the mean radius of the Earth; $f=2\Omega\sin(\phi)$ is the Coriolis parameter; p_s is the surface pressure; $\dot{T}$ is the diabatic heating; c_p is the specific heat of dry air; R_d is the specific gas constant for dry air; q is the water vapor specific humidity; $\dot{q}$ is the humidity tendency from condensation and surface fluxes; the F terms encompass nonconservative momentum effects like friction; square brackets indicate the zonal mean; and primes indicate deviations from the zonal mean. In a hybrid-sigma coordinate system, the surface pressure tendency due to eddies has a special form, described in the appendix.

Because an axisymmetric simulation has no zonal asymmetries, the governing equations in this case result from dropping all terms with primed quantities,

$$\frac{\partial[u]}{\partial t}+\frac{[v]}{a\cos(\phi)}\frac{\partial}{\partial\phi}\left([u]\cos(\phi)\right)+[\omega]\frac{\partial[u]}{\partial p}-f[v]=[F_\lambda] \tag{11}$$

$$\frac{\partial[v]}{\partial t}+\frac{[v]}{a}\frac{\partial[v]}{\partial\phi}+[\omega]\frac{\partial[v]}{\partial p}+f[u]+\frac{[u]^2\tan(\phi)}{a}+\frac{1}{a}\frac{\partial[\Phi]}{\partial\phi}=[F_\phi] \tag{12}$$

$$\frac{\partial[T]}{\partial t}+\frac{[v]}{a}\frac{\partial[T]}{\partial\phi}+[\omega]\frac{\partial[T]}{\partial p}-\frac{R_d[T][\omega]}{c_p p}=[\dot{T}] \tag{13}$$

$$\frac{\partial [p_s]}{\partial t} = -\int_0^{p_s} \nabla \cdot [\vec{v}_H][p]\mathrm{d}p \tag{14}$$

$$\frac{\partial [q]}{\partial t} + \frac{[v]}{a}\frac{\partial [q]}{\partial \phi} + [\omega]\frac{\partial [q]}{\partial p} = [\dot{q}] \tag{15}$$

It is self-evident that the circulation in the axisymmetric simulation will substantially deviate from the eddy-permitting simulation because the balance of terms differs. However, it is unclear which eddy terms are most important for transforming the zonal-mean climate from the axisymmetric state to the eddy-permitting state. Quasigeostrophic eddy fluxes of zonal momentum and heat ($[u'v']$ and $[v'T']$) are the dominant eddy terms in the extratropical free atmosphere (Andrews et al., 1987), but we will critically examine their contributions to the tropical and subtropical atmosphere. Here, "quasigeostrophic" refers to the fact that these eddy fluxes are the only eddy fluxes present in the zonal-mean primitive equations scaled for quasigeostrophic motion in a shallow atmosphere (Edmon et al., 1980).

In this study, we selectively apply the zonal-mean, time-mean tendencies of momentum, heat, mass, and moisture due to eddy flux convergences calculated from the eddy-permitting simulation to the axisymmetric simulation as zonal-mean tendencies in each of the above equations. For example, comparing equation (11) to equation (6), it can be seen that

$$\overline{[E_\lambda]} = -\frac{1}{a\cos^2(\phi)}\frac{\partial}{\partial \phi}\left(\overline{[u'v']}\cos^2(\phi)\right) - \frac{\partial \overline{[\omega' u']}}{\partial p} \tag{16}$$

where $\overline{[E_\lambda]}$ is the time-mean, zonal-mean zonal momentum tendency due to the eddies, and the overbar indicates the time mean. The zonal and meridional momentum, heat, and moisture tendencies due to the eddy flux convergences in the eddy-permitting simulation and applied to the axisymmetric simulations are shown in Figure 4. Eddy flux convergences are calculated online in the model at every time step, because we found that substantial errors occur if they are calculated in postprocessing. Unlike the similar axisymmetric scheme in Kushner and Polvani (2004), we explicitly calculate all eddy terms. Our method seems numerically stable in the tropics, as well, although this may simply be due to the use of a more comprehensive model.

Here we will summarize the basic structure of eddy transport in the model. Eddies remove easterly momentum from the midlatitudes and deposit it in the subtropics, resulting in an effective transport of positive zonal momentum from the subtropics to the midlatitudes (Figure 4a). This transport is dominated by the quasigeostrophic eddy fluxes, except at the jet level where the vertical eddy flux convergence is as large as the horizontal eddy flux convergence.

Similarly, the eddies transport equatorward momentum out of the midlatitudes and into the subtropics (Figure 4b). This acts to decelerate (accelerate) the poleward (equatorward) flow in the Hadley cell and vice versa in the Ferrel cell. The metric term, $[u'^2]\tan(\phi)/a$, becomes dominant toward the pole and especially in the stratospheric jet. While the magnitude of the meridional momentum tendencies is larger than the magnitude of the zonal momentum tendencies, the dominant terms in the meridional momentum equation are an order of magnitude larger than those in the zonal momentum equation. Meridional momentum balance is primarily zonal geostrophy, and hence, the contribution of these eddy tendencies to the total meridional momentum balance is relatively small.

Eddies remove heat from the subtropics and transport it poleward and upward, with some additional heat flux convergence into the stratospheric jet (Figure 4c). Eddy moisture transport is concentrated at the surface and is dominated by the vertical transport of moisture from the surface to the midtroposphere (Figure 4d). Vertical moisture gradients are far larger than horizontal moisture gradients, so minor vertical eddy motions can drive large moisture transports, and there is little moisture transport above the midtroposphere due to the strong exponential decrease of moisture with height. Eddies also transfer mass from the poles to the subtropics, driving a positive tendency in surface pressure in the subtropics and a negative tendency in surface pressure in the extratropics (Figure 5).

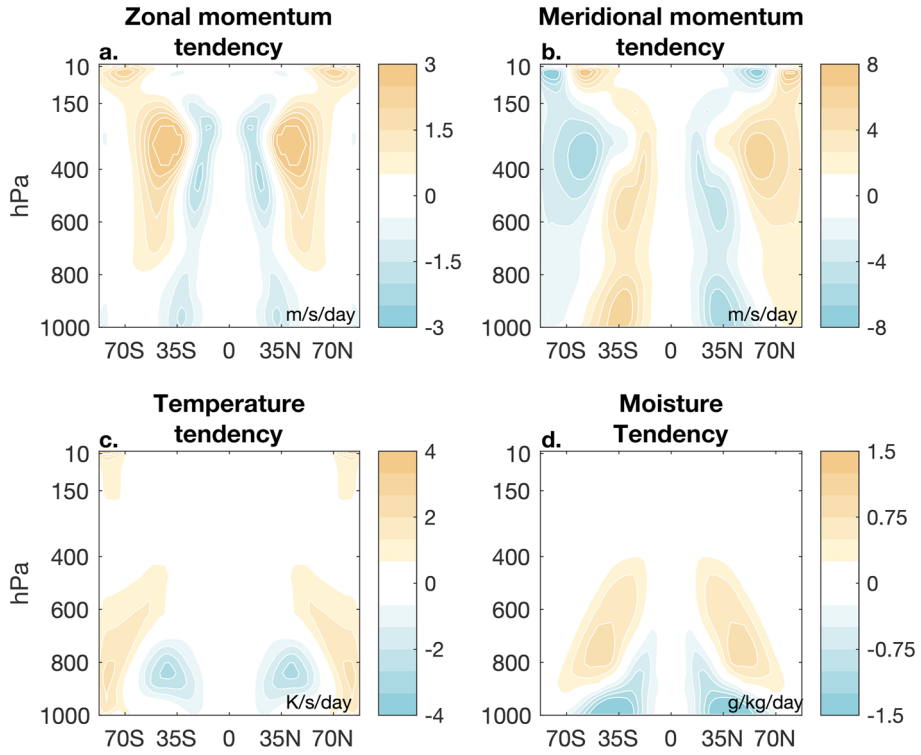

Figure 4. Tendencies of (a) zonal momentum ($-\partial_y[u'v'] - \partial_p[\omega' u']$), (b) meridional momentum ($-\partial_y[v'v'] - \partial_p[\omega' v'] - [u'^2]\tan(\phi)/a$), (c) temperature ($\partial_y[v'T'] - \partial_p[\omega' T'] + (R[\omega' T'])/(c_p p)$), and (d) moisture ($-\partial_y[v'q'] - \partial_p[\omega' q']$) due to eddy flux convergences and eddy processes in the eddy-permitting simulation in gray radiation aquaplanet model.

The bulk formulas for surface fluxes in the zonal mean are proportional to the zonal-mean surface wind speed. Though it is not intuitive, eddies contribute to the zonal-mean surface wind speed and hence the zonal-mean surface fluxes. This can be seen through a Reynolds decomposition of the zonal-mean surface wind speed,

$$\left[|\vec{v}_s|\right] = \left[\sqrt{u_s^2 + v_s^2}\right] = \left[\sqrt{[u_s]^2 + [v_s]^2 + 2\left([u_s]u_s' + [v_s]v_s'\right) + u_s'^2 + v_s'^2}\right] \tag{17}$$

where u_s and v_s are the zonal and meridional surface winds and $\vec{v}_s$ is the surface wind vector. The radical is situated inside the zonal mean operator, so the nonlinear terms do not vanish and the eddy terms cannot be separated from the mean flow terms. As the zonal-mean surface fluxes are the result of the covariance between the surface wind speed, the variable of interest, and the drag coefficient, which itself is a function of the local atmospheric state, calculating the surface fluxes due to the eddies directly from the bulk formulas and Monin-Obukhov theory is intractable. In lieu of a more complete theory for eddy influences on surface fluxes of heat, moisture, and momentum, we instead calculate both the zonal-mean surface fluxes and the surface fluxes based on zonal-mean quantities online in the eddy-permitting simulation and take the difference to estimate the fluxes due to the eddies, shown in Figure 6. These surface fluxes are applied as time-mean, zonal-mean contributions to the surface energy, moisture, and momentum budgets and are propagated into the atmosphere by the boundary layer scheme. The relative contribution of the eddies to each of the surface fluxes varies by region and variable. In the extratropics, eddies contribute up to 80% of the northward surface stress and 40% of the westward surface stress, while in the tropics they con-

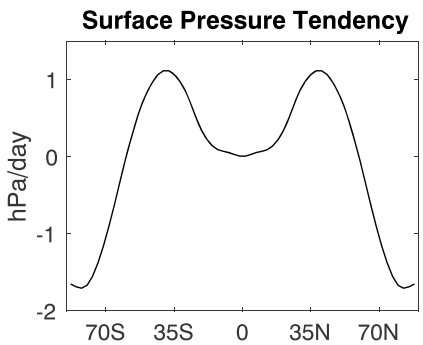

Figure 5. Tendency of surface pressure due to eddy flux convergences ($-\int_0^{p_s} \nabla \cdot [v'p']\mathrm{d}p$) in the eddy-permitting simulation in gray radiation aquaplanet model.

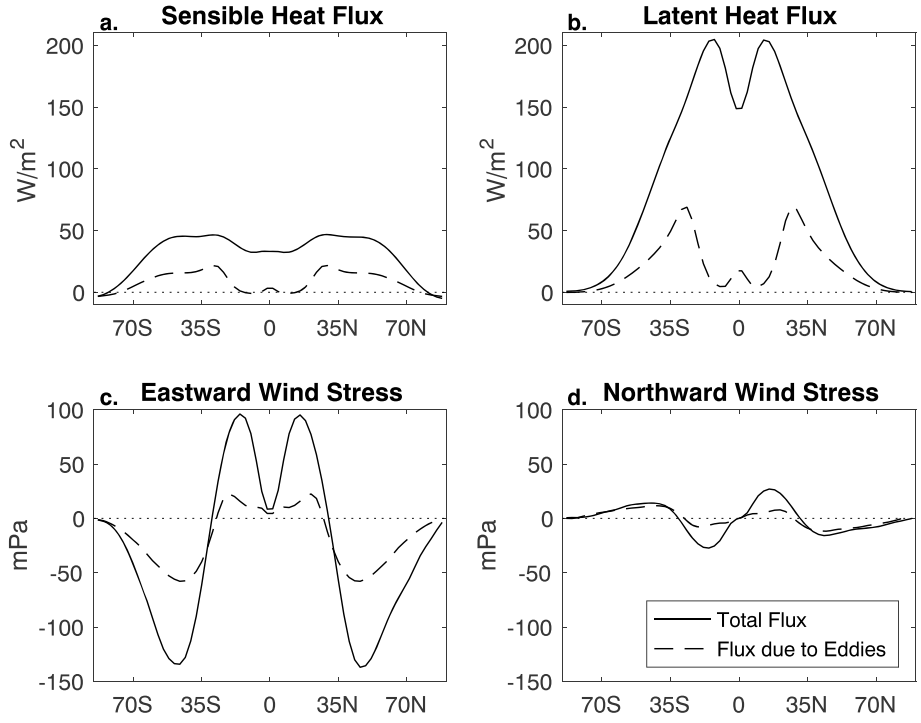

Figure 6. Zonal-mean surface fluxes of (a) sensible heat and (b) latent heat and surface (c) eastward and (d) northward wind stress in solid, with the part associated with eddies in dashed. See text for details.

tribute less. The eddies' contribution to surface fluxes of heat and moisture is approximately 30% in the extratropics and zero in the tropics, with a maximum in the subtropics where the zonal-mean surface wind speeds are close to zero.

Finally, we apply the large-scale temperature and humidity tendencies due to large-scale condensation driven by the eddies. Midlatitude Rossby waves support the development of frontal cyclones, with sharp temperature gradients between the cold and warm sectors. At the cold and warm fronts, warm sector air, rich with moisture, is lofted over the cold sector air. It cools as it rises and eventually condenses, forming large-scale stratus precipitation. In the net, one would expect enhanced large-scale precipitation in these storm track latitudes.

This behavior cannot be described by zonal-mean eddy flux convergences of temperature and humidity, as it can only be produced in the presence of zonal asymmetries. To estimate these tendencies, we first run the axisymmetric simulation with all other forcings (e.g., Figures 4–6) applied. We then take the difference in large-scale condensational temperature and humidity tendencies between this simulation and the eddy-permitting simulation. Applying the resulting difference as temperature and humidity tendencies to the axisymmetric simulation seems to overprescribe the effect of the eddies on large-scale condensation, as there seems to be a mean flow feedback that amplifies any prescribed storm track diabatic heating and drying/wetting. The feedback could be related to the vertical gradient of the humidity tendency, which amplifies the existing vertical humidity gradient. Regardless of the cause of this amplification, we instead apply 50% of the difference between the eddy-permitting and axisymmetric simulations as a rough estimate of the eddy effect on large-scale condensation (Figure 7). These eddy effects are an amplification of large-scale storm track condensation, with enhanced condensation in the midtroposphere, enhanced evaporation of rain in the lower troposphere, and little net impact on the total moist enthalpy.

4. Results

Having documented the climate of GRAM, we now explore the role of eddies in shaping the Hadley circulation. Figure 8 displays the zonal-mean climate of GRAM in eddy-permitting, pure axisymmetric, and eddy-forced axisymmetric simulations. It is surprising that the Hadley cell is confined to the tropical upper troposphere in the axisymmetric simulation, as axisymmetric cells in previous studies bear some resem-

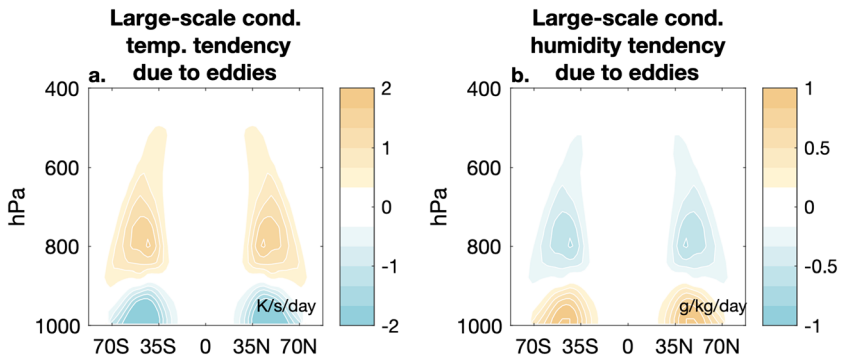

Figure 7. Zonal-mean effect of eddies on (a) temperature and (b) humidity tendencies due to large-scale condensation.

blance to the observed Hadley cells. Further, the Hadley cell strength is nearly equal in the eddy-permitting and axisymmetric simulations, which also differs from previous studies (Becker et al., 1997; Kim & Lee, 2001; Walker & Schneider, 2005). However, because the meridional wind is a function of the vertical derivative of the stream function, the meridional winds are far stronger in the axisymmetric simulation. The subtropical jet is also substantially stronger in the axisymmetric simulation, though weaker than what would be expected from true angular momentum conservation due to hyperdiffusion. There is a polar cell at the surface, but it is associated with vertical diffusion in the boundary layer. We will return to this curious circulation later.

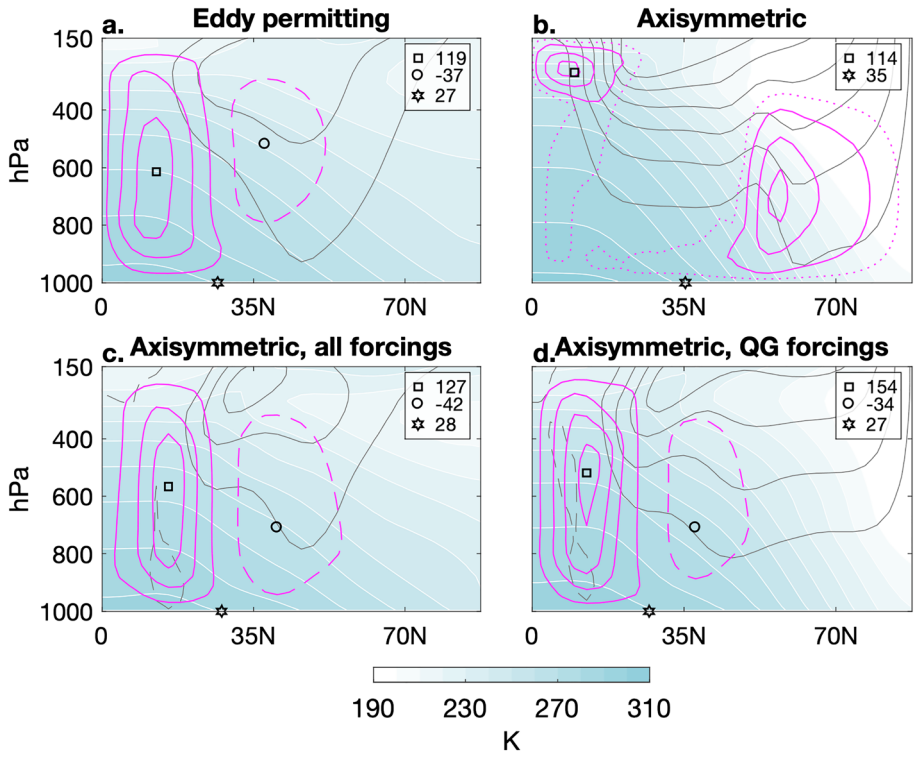

Figure 8. Zonal-mean climate of gray radiation aquaplanet model (a) in the eddy-permitting simulation, (b) in the pure axisymmetric simulation, (c) in the axisymmetric simulation with all eddy forcings applied, and (d) in the axisymmetric simulation with only quasigeostrophic eddy forcings applied. (shading) Temperature every 10 K, (black contours) zonal-mean zonal wind every 10 m/s, and (magenta contours) mean meridional stream function every 40 $\times 10^9$ kg/s starting from 20 $\times 10^9$ kg/s. Negative zonal-mean zonal wind and mean meridional stream function indicated by dashed contours. The location of the stream function maximum and minimum are indicated by the square and circle, respectively, and the edge of the Hadley circulation is indicated by a star. The 5 $\times$ 10^9 kg/s contour is dotted in the pure axisymmetric simulation.

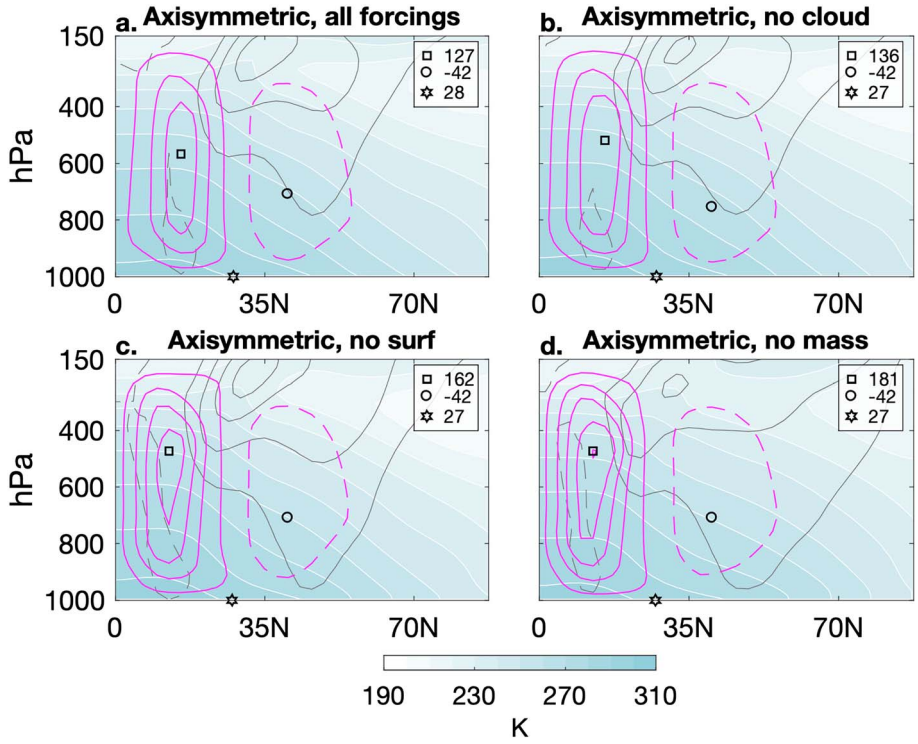

Figure 9. As in Figure 8, but for the zonal-mean climate of gray radiation aquaplanet model (a) in the axisymmetric simulation with all eddy forcings applied, which is the same as Figure 8c, (b) in the axisymmetric simulation with all eddy forcings except large-scale condensation, (c) in the axisymmetric simulation with all eddy forcings except surface fluxes, and (d) in the axisymmetric simulation with all eddy forcings except surface pressure.

In the axisymmetric simulation with all eddy forcings, the Hadley and Ferrel cells are of similar strength and structure to those in the eddy-permitting simulation, as are the zonal winds. Considering the difficulty in accounting for the impacts of the eddies on five different physical fields, it is reasonable to conclude that the zonal-mean general circulation is a robust solution to a given set of external forcings and eddy forcings.

If the axisymmetric simulation is forced only with quasi-geostrophic forcings (e.g., the meridional convergences of zonal momentum and heat), the qualitative structure of the eddy-permitting simulation is still reproduced. However, the Hadley cell is 25% stronger, with the maximum stream function value shifted upward by 100 hPa, and the zonal winds are nearly 100% stronger. While quasigeostophic eddy effects can deepen the Hadley cell, produce a Ferrel cell, and weaken the zonal winds, a full accounting of the non-quasigeostrophic eddy effects, including vertical fluxes, surface fluxes, and convection impacts, is necessary to replicate the general circulation.

Beyond vertical and other nonquasigeostrophic eddy fluxes, the eddy impacts on surface fluxes, surface pressure, and large-scale condensation are also important. Neglecting to apply the eddy condensation forcings results in a slightly stronger Hadley cell and slightly stronger zonal winds, potentially owing to the stronger subtropical meridional temperature gradient (Figure 9b; Adam et al., 2014). However, failing to account for the eddy impact on surface fluxes or the eddy impact on surface pressure has a similar impact on the circulation as only applying the quasigeostrophic eddy fluxes. A simple explanation is that the eddies and the Hadley cells constructively interact to redistribute heat, momentum, and mass. Therefore, failing to account for the eddy impacts on a given field will necessitate that the Hadley circulation "picks up the slack."

For example, without the eddy impact on surface fluxes accounted for, the Hadley cells must intensify to dissipate the same amount of momentum in the tropics. Surface stresses due to eddy and zonal-mean zonal winds both act to dissipate (generate) interior atmospheric momentum in the midlatitudes (tropics). With the eddy impact accounted for, the surface zonal-mean zonal winds do not need to be as strong, and through the Coriolis torque the surface zonal-mean meridional winds do not need to be as strong, to dissipate a given amount of momentum. Given that the axisymmetric simulation with all eddy forcings applied remains

slightly stronger than the eddy-permitting simulation (Figure 8), there may yet be other eddy impacts we have overlooked or have been unable to accurately reproduce because they are interactive, such as convective processes.

4.1. Vertically Integrated Heat Budget

To elucidate the underlying physical mechanisms for the difference in behavior between the axisymmetric and eddy-permitting simulations, we examine the simulations' vertically integrated heat and momentum budgets. In the time-mean, the vertically integrated heat budget in flux form is given by

$$R = [SH_{\text{mean}}] + [SH_{\text{eddy}}] + c_p \left\{ \left\langle [\dot{T}_{\text{rad}}] \right\rangle + \left\langle [\dot{T}_{\text{conv,mean}}] \right\rangle + \left\langle [\dot{T}_{\text{conv,eddy}}] \right\rangle - \frac{1}{a\cos(\phi)} \left\langle \frac{\partial}{\partial \phi} [v'T'] \cos(\phi) \right\rangle - \frac{1}{a\cos(\phi)} \left\langle \frac{\partial}{\partial \phi} [v][T] \cos(\phi) \right\rangle + \frac{R_d}{c_p} \left\langle \frac{[\omega'T']}{p} \right\rangle + \frac{R_d}{c_p} \left\langle \frac{[\omega][T]}{p} \right\rangle + \left\langle [\dot{T}_{\text{damping}}] \right\rangle \right\} \tag{18}$$

where R is the budget residual, SH_{mean} and SH_{eddy} are the sensible heat fluxes in the zonal mean and due to the eddies, $\dot{T}_{\text{rad}}$ is the radiative heating (which is dominated by longwave cooling), $\dot{T}_{\text{conv,mean}}$ and $\dot{T}_{\text{conv,eddy}}$ are the condensational heating in the zonal mean and due to the eddies, and $\dot{T}_{\text{damping}}$ is the damping due to hyperdiffusion. Angled brackets indicate the vertical integral, defined as

$$\langle \chi \rangle = \frac{1}{g} \int_0^{p_s} \chi \, dp \tag{19}$$

where g is the acceleration due to gravity, p_s is the surface pressure, and χ is any term in the budget equation. The units of the budget are in watts per square meter.

We will refer to the $[v'T']$ and $[v][T]$ terms as the eddy and mean heat flux convergence and will refer to the $[\omega'T']$ and $[\omega][T]$ terms as the eddy and mean adiabatic heating. The mean flow terms describe the effects of the Hadley and Ferrel cells.

In the tropics and subtropics the dominant heat balance in the axisymmetric simulation is between convective heating and radiative cooling, with smaller contributions from the Hadley cell via mean heat flux convergence and mean adiabatic cooling (Figure 10b). By contrast, in the eddy-permitting simulation convective heating and heat flux convergence by the mean flow is balanced by both mean adiabatic cooling and radiative cooling (Figure 10a). The mean heat flux convergence and adiabatic cooling in the subtropics are almost twice as strong in the eddy-permitting simulation as they are in the axisymmetric simulation.

While the Hadley cell fluxes dry static energy poleward (Frierson, Held, et al., 2007), it fluxes *heat* from the subtropics to the tropics in all simulations (Figure 10; and also see Becker et al., 1997). Consider the heat flux by the mean flow, $[v][T]$. Aloft, poleward flow occurs at low temperatures while at the surface, equatorward flow occurs at high temperatures. Assuming the depth of the poleward and equatorward flow is similar, the vertical integral will be weighted toward the equatorward flow by virtue of it occurring at high temperatures, and hence, the heat flux will be equatorward. However, the Hadley cell cools the tropics and warms the subtropics through adiabatic subsidence more than it warms the tropics and cools the subtropics through meridional heat flux convergence. If one considers the heat transport by the cell as the sum of meridional transport and adiabatic warming/cooling, then the cell effectively transports heat from the tropics to the subtropics. Note that "heat" specifically means c_pT, or enthalpy.

Unlike Becker et al. (1997), we do not find such an obvious transition from radiative to eddy-driven subsidence as radiative cooling remains the dominant heat dissipation mechanism in the subtropics. It could be the case that the increase in Hadley cell heat transport is due to the additional subtropical cooling by the eddies, but we also note that unlike the model examined in Becker et al. (1997), GRAM includes latent heating effects, which are a first-order process (Figure 10, "$\dot{T}_{\text{conv,mean}}$"), and a more sophisticated treatment of radiation. However, Trenberth and Stepaniak (2003) note that poleward eddy heat transport effectively redistributes subtropical radiative cooling poleward. Indeed, we see that the radiative cooling weakens in the subtropics with the introduction of eddies (compare Figures 10a and 10b). It therefore seems reasonable to argue that the eddies reduce the efficiency with which subtropical radiative cooling drives Hadley cell subsidence.

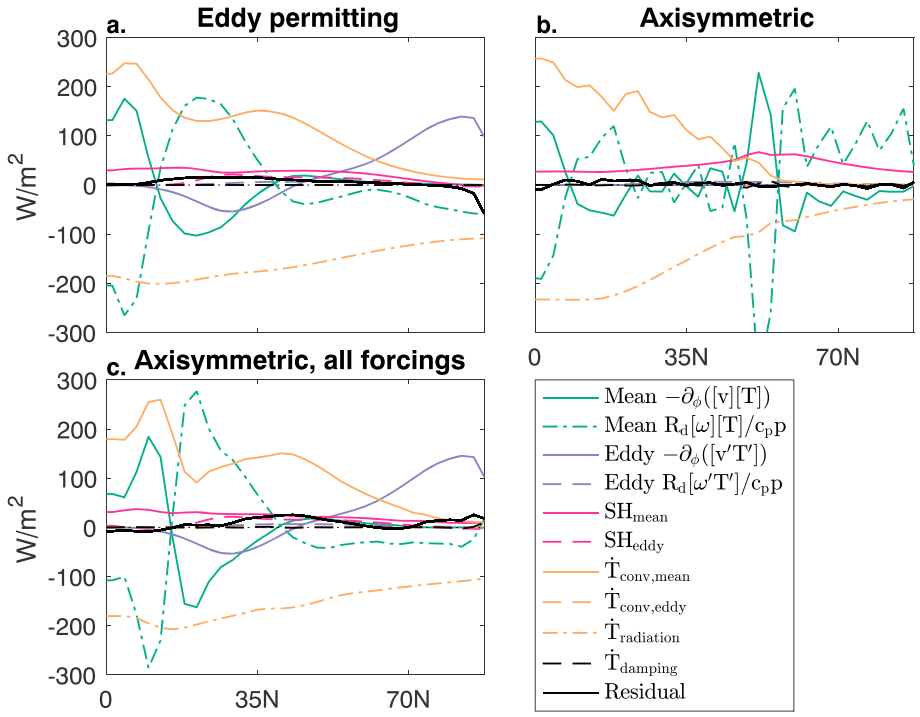

Figure 10. Vertically integrated heat budget of gray radiation aquaplanet model in (a) the eddy-permitting simulation, (b) the pure axisymmetric simulation, and (c) the axisymmetric simulation forced with eddy tendencies. See text for definitions of each term.

The vertically integrated geopotential flux, the other component of the dry static energy flux, will be poleward, as poleward flow occurs at high geopoential and equatorward flow occurs at low geopotential. This must be larger than the equatorward heat flux to guarantee that the Hadley cell fluxes dry static energy poleward. The Hadley cell can therefore be viewed as a potential energy transport mechanism. If one were to consider potential temperature instead of heat, similar to the dry static energy, one would find that the Hadley cell fluxes potential temperature poleward (in part because potential temperature is nearly equivalent to dry static energy, with some caveats; see DeCaria, 2006).

Beyond the tropics, the midlatitude heat balance in the eddy-permitting simulation is between surface flux and convective heating and longwave cooling, whereas at the pole longwave cooling is balanced by eddy heat flux convergence. In the axisymmetric simulation there is a couplet of mean adiabatic cooling/warming and heat flux convergence/divergence reflecting the thermally direct polar cell.

The radiative cooling is slightly stronger in the axisymmetric simulation in the tropics. Elsewhere it is substantially weaker in the axisymmetric simulation, reflecting colder extratropical temperatures. Some of the reduction in extratropical temperatures is due to the absence of eddy heat transport, but in the absence of storm tracks there is also no large-scale condensational heating in the extratropics. The meridional heat transport in the axisymmetric simulation is weaker than in the eddy-permitting simulation because the cell occupies a narrower altitude range. In the axisymmetric cell, the temperatures in the upper and lower branches of the cell are similar, whereas in the deeper cell in the eddy-permitting simulation, the temperatures in the lower branch are substantially higher than those in the upper branch, so the vertically integrated flux is larger.

There are some minor differences between the heat budgets of the eddy-permitting simulation and the axisymmetric simulation with all eddy forcings applied. In the tropics, the peak values of convective heating and mean adiabatic cooling are weaker, and while the basic balance of terms is essentially the same, the features are generally sharper.

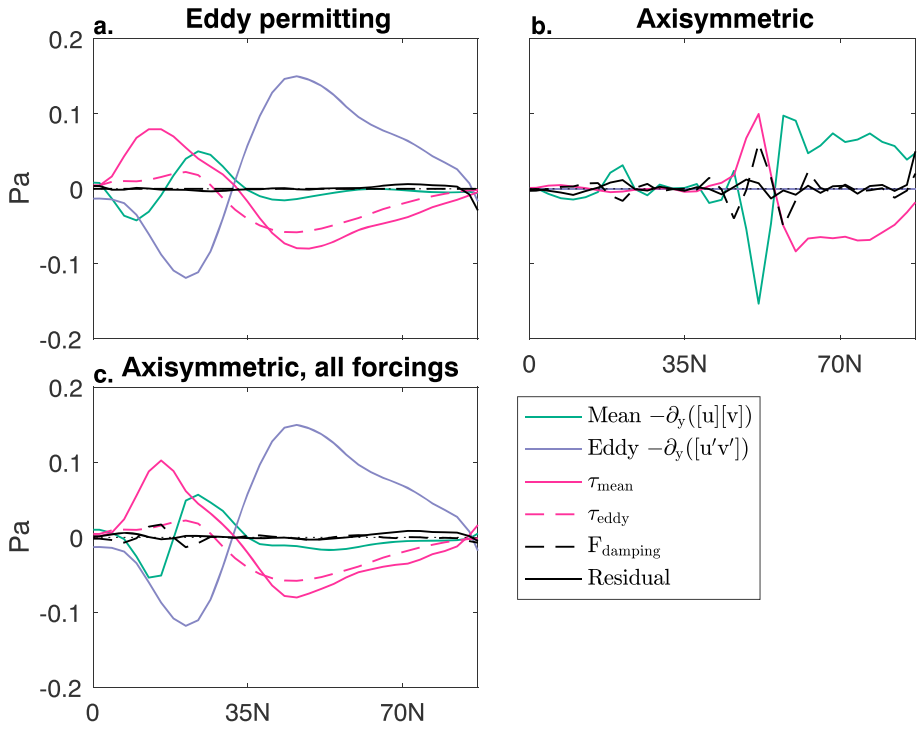

Figure 11. As in Figure 10 but for the vertically integrated momentum budget. See text for definitions of each term.

4.2. Vertically Integrated Zonal Momentum Budget

In the time mean, the vertically integrated zonal momentum budget is given by

$$R = \tau_{x,\text{mean}} + \tau_{x,\text{eddy}} - \frac{1}{a\cos^2(\phi)}\left\langle \frac{\partial}{\partial\phi}\left([u'v']\cos(\phi)\right)\right\rangle - \frac{1}{a\cos^2(\phi)}\left\langle \frac{\partial}{\partial\phi}[u][v]\cos\phi)\right\rangle + \left\langle [F_{\text{damping}}]\right\rangle \quad (20)$$

where $\tau_{x,\text{mean}}$ and $\tau_{x,\text{eddy}}$ are the surface zonal wind stresses due to the mean flow and due to eddies, F_{damping} is the damping, and the budget units are in pascals. We will refer to the $[u'v']$ and $[u][v]$ terms as the eddy and mean momentum flux convergence.

In the eddy-permitting simulation in the tropics, the surface wind stress acts to accelerate the flow against mean and eddy momentum flux divergence, whereas in the midlatitudes, the surface wind stress dissipates the convergence of momentum by the eddies (Figure 11). There is some compensation in the subtropics between eddy momentum flux divergence and mean momentum flux convergence. As a result the latitude of zero surface wind stress is displaced slightly equatorward of the latitude of zero eddy momentum flux convergence. This three-way balance between the surface stress, the eddy momentum flux divergence, and mean momentum flux convergence may be one reason why the latitude of zero surface zonal wind is not a perfect proxy for the Hadley cell edge, especially in the winter months when the momentum flux by the mean flow is strongest (Waugh et al., 2018). The momentum budget is nearly identical between the eddy-permitting and axisymmetric simulations with all eddy forcings, except that the latter has a large dipole of damping in the subtropics. This could be indicative of persistent instabilities in the simulation, which may also be manifest in the sharp structures in the momentum and heat budgets (Figures 10 and 11).

In the axisymmetric simulation, there is vanishingly weak momentum transport in the Hadley cell that is balanced primarily by damping. This can be visually confirmed by noting that the zonal-mean zonal wind speeds are essentially the same in the regions of poleward and equatorward flow (Figure 8), that is, the poleward momentum flux aloft is nearly compensated by the equatorward momentum flux below. In the polar cell, the mean momentum flux convergence is balanced by wind stress, with nonnegligible damping potentially indicative of instabilities.

5. Discussion

Our finding that an axisymmetric Hadley cell only exists in the upper troposphere with vanishingly weak momentum transport seems to contradict other studies (see, e.g., Becker et al., 1997; Held & Hou, 1980; Kim & Lee, 2001). There are numerous differences in the physics implementations between GRAM and the models used in these other studies that could lead to this discrepancy. We will focus on two possibilities: the method and strength of numerical damping and convection.

Viscosity is often included in axisymmetric models to damp numerical instabilities, and it typically needs some finite minimum value (Held & Hou, 1980; Kim & Lee, 2001). Here, we instead ran the model with hyperdiffusion and an aggressive time step. The polar cell present in the axisymmetric simulations exists within the boundary layer where there is vertical diffusion, so it may be the case that vertical diffusion is necessary for the Hadley cell to extend to the surface. To test whether viscosity drives the transition from zero to nonzero momentum transport in an axisymmetric Hadley cell, we add a diffusion term to the zonal and meridional momentum, water vapor, and thermodynamic equations and disable hyperdiffusion. As an example, for the axisymmetric zonal momentum equation in flux form, we have

$$\frac{\partial [u]}{\partial t} + \frac{1}{a\cos(\phi)}\frac{\partial}{\partial \phi}\left([u][v]\cos(\phi)\right) + \frac{\partial}{\partial p}\left([u][\omega]\right) - f[v] = [F_\lambda] + \frac{\partial}{\partial p}\left(\nu(\rho g)^2 \frac{\partial [u]}{\partial p}\right) \tag{21}$$

where ν is the diffusion coefficient (units of square meters per second, for ease of reference to Held & Hou, 1980, and other studies), and ρ is the density. When we switch from hyperdiffusion to a standard value of $\nu = 1.0\ \mathrm{m}^2/\mathrm{s}$ viscosity in the pure axisymmetric simulation, the Hadley cell extends down to the surface (Figure 12) and fluxes momentum poleward. We also find that increasing viscosity increases the intensity of the circulation and drives it further from angular momentum conservation, consistent with Held and Hou (1980), Becker et al. (1997), Kim and Lee (2001), and Adam and Paldor (2010). Is viscosity driving a regime change in the circulation?

5.1. An Inviscid Hadley Cell

As in Held and Hou (1980), consider an axisymmetric Boussinesq fluid on the sphere in the time mean. The zonal-mean angular momentum budget is given by

$$[\vec{v}] \cdot \nabla [M] = \tau_x + a\cos(\phi)\frac{\partial}{\partial z}\left(\nu \frac{\partial [u]}{\partial z}\right) \tag{22}$$

where τ_x is the zonal surface wind stress, $[\vec{v}] = ([v], [w])$, and $M = a\cos(\phi)(u + \Omega a \cos(\phi))$ is the angular momentum per unit mass. We will consider $\tau_x = 0$ for $z > 0$ and, for now, consider an inviscid atmosphere with $\nu = 0$. Held and Hou (1980) show [v]=[w]=0 is one possible solution. Here, we ask if it is possible for a Hadley cell to reach the surface in such an atmosphere?

At $z = 0$, we require that $[w] = 0$ and $\nu = 0$ (as viscosity is internal). Therefore, the budget reduces to

$$\frac{[v]}{a\cos(\phi)}\frac{\partial [M]}{\partial \phi} = \tau_x \quad \text{at z = 0} \tag{23}$$

To ensure that the circulation is inertially stable, we also require $[M]$ to decrease toward the pole. As we are considering a Hadley cell, we will also only consider equatorward surface [v].

With these two constraints, the advection term is positive in both hemispheres, so the frictional term must also be positive, which demands surface easterlies.

If we take the integral of the flux form of equation (22) in the area bounded by the Hadley cell, we find a contradiction, with a net frictional source of momentum and no sink,

$$\iint \nabla \cdot \left([\vec{v}][M]\right) \mathrm{d}A = \oint \left([\vec{v}][M]\right) \cdot \hat{n} \mathrm{d}l = 0 \tag{24}$$

$$\iint \tau_x \mathrm{d}A \geq 0 \tag{25}$$

where $\mathrm{d}l$ is the path of the $\Psi = 0$ contour and $\hat{n}$ is the unit normal to the $\Psi = 0$ contour. As the flow is everywhere parallel to the stream function contour, $[\vec{v}][M]$ is perpendicular to $\hat{n}$, so the dot product of the two is zero, and hence, the integral of the advective terms is zero.

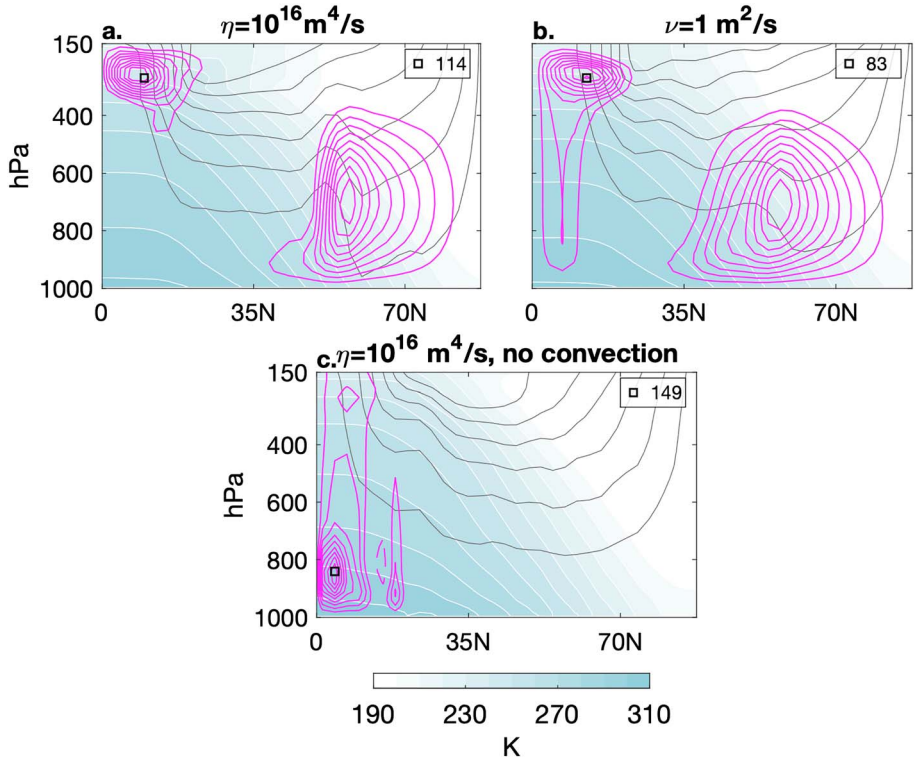

Figure 12. As in Figure 3, but for the zonal-mean climate of gray radiation aquaplanet model (a) in the pure axisymmetric simulation with hyperdiffusion coefficient 1 $\times 10^{16}$ m^4/s, (b) in the pure axisymmetric simulation with a viscosity of 1 m^2/s and no hyperdiffusion, (c) in the pure axisymmetric simulation with hyperdiffusion coefficient 1 $\times 10^{16}$ m^4/s, no large-scale condensation, and a 2-day convective relaxation timescale. The roughness length has been increased by a factor of ten over the other simulations, otherwise irregular boundary layer circulations dominate. Stream function contours as in Held and Hou (1980): every 0.1 of the maximum stream function value.

We would not have a contradiction for two specific cases: the trivial solution with $[v] = 0$ at the surface and no column-integrated angular momentum transport, or the solution with nonzero viscosity. For the former, we can note the trivial solution of equation (23) with $\tau_x = 0$ and take the vertical integral of the flux form of equation (22) and find

$$\left\langle \frac{1}{a\cos(\phi)} \frac{\partial}{\partial \phi} \left([v][M]\cos(\phi) \right) \right\rangle = \langle \tau_x \rangle = 0 \tag{26}$$

where the angled brackets indicate the vertical integral as before. Thus, there is no contradiction so long as there is no surface circulation and no column-integrated momentum transport.

If we allow nonzero viscosity, the area integral becomes

$$\iint \tau_x \mathrm{d}A = -\iint a\cos(\phi) \frac{\partial}{\partial z} \left(\nu \frac{\partial [u]}{\partial z} \right) \mathrm{d}A \tag{27}$$

That is, a viscous sink balances a frictional source of angular momentum. One can illustrate these same conclusions if the integrals and balances are evaluated along a contour of constant Ψ in contact with the surface. Substituting the meridional eddy momentum flux convergence or hyperdiffusion for vertical diffusion in the preceding derivation will lead to the same conclusion—that some negative tendency of angular momentum is needed within the interior of the circulation if it is to extend down to the surface.

We conclude that the Hadley cells in an inviscid axisymmetric atmosphere with nonzero surface drag cannot extend down to the surface nor flux momentum poleward. Williams (2003) seemingly demonstrates the contrapositive: that in an axisymmetric atmosphere with zero surface drag but vanishing hyperdiffusion, the Hadley cells *do* extend to the surface. However, our axisymmetric simulation is akin to the nearly inviscid limit of Held and Hou (1980) because it uses hyperdiffusion, an internal stress analogous to viscosity in the

preceding derivation. Why then, does our circulation not extend over the depth of the troposphere as one might expect? We can provide two plausible explanations.

First, our hyperdiffusive damping is effectively orders of magnitude weaker than the viscosities typically used in axisymmetric studies. If we assume a characteristic height, H, of 10 km and meridional length, L, of 3,000 km for the Hadley cell, the scaling between the viscosity coefficient and the hyperdiffusion coefficient, η, for nth-order hyperdiffusion is

$$\frac{\nu}{H^2} \propto \frac{\eta}{L^n} \tag{28}$$

For $\eta = 1 \times 10^{16}$ m^4/s used here, the corresponding viscosity is 0.01 m^2/s, substantially lower than values on the order of 1–10 m^2/s used in many axisymmetric simulations. However, we find this answer unsatisfactory as it still seems to contradict the nearly inviscid theoretical result of Held and Hou (1980).

A second plausible explanation is that convection prevents the nearly inviscid cell from descending below the upper troposphere. Indeed, when we disable large-scale convection and octuple the convective relaxation time to 2 days, the Hadley cell deepens and reaches the surface (Figure 12c).

We hypothesize that it is the interaction of convection with the Ferrel cell, rather than the Hadley cell that ultimately drives the axisymmetric Hadley cell into the upper troposphere. At low viscosities, Held and Hou (1980) note the development of a small Ferrel cell at the poleward-tilting edge of the Hadley cell. Vertical diffusion undoubtedly transfers westerly momentum from the Hadley cell to the Ferrel cell, where it can then be dissipated by friction at the surface in poleward flow. However, if convection is sufficiently fast so as to keep the temperature gradient close to its equilibrium value, the Ferrel cell may cease to exist because it cannot homogenize angular momentum.

Wirth and Dunkerton (2006) find that the thermal relaxation timescale does indeed drive regime behavior in axisymmetric simulations. While a long timescale produces monsoon-like (or equivalently, Hadley-cell-like) circulations, with weak winds and temperatures far from their equilibrium, a short timescale characteristic of vigorous convection leads to hurricane-like circulations with strong winds and temperatures close to their equilibrium. This suggests that convection may "kill off" the Ferrel cell by preventing it from modifying the equilibrium temperature gradient, thereby eliminating the primary dissipation mechanism for poleward angular momentum transport in the Hadley cell.

If the Hadley cell descends below jet level, it will flux momentum poleward. By virtue of thermal wind shear, the poleward flow aloft will occur in a region of strong meridional shear, whereas the equatorward flow at the surface will occur in a region of weak meridional shear, so that in the net, the transport has to be poleward. Therefore, without a Ferrel cell, a nearly inviscid Hadley cell may not be able to descend below jet level because there is no mechanism to dissipate the inevitable momentum transport.

There seems to be some minimum internal stress necessary to support the development of a surface circulation (Figure 12b), evidence that the inviscid limit in a moist convecting atmosphere differs from the inviscid limit in a dry, nonconvecting atmosphere.

5.2. Summary

Vertical diffusion and horizontal hyperdiffusion are parameterizations of diffusive transport by unresolved eddies, so if these terms are not vanishingly small in axisymmetric simulations one might underestimate the impact of eddies on the basic structure of the circulation. As we have shown, the typical viscosities used in previous axisymmetric models are relatively large and leave a diminished role for the eddies in shaping the structure of the circulation. More importantly, hyperdiffusion, vertical diffusive transport, and resolved eddy momentum transport all function to deepen the Hadley cell. While vertical diffusion can mimic the effects of cumulus friction in the tropics (e.g., Stone et al., 1974), it seems to be the case that diffusion has its greatest impact on the circulation in the subtropics (where there is little convective mixing).

Viscous models can be useful for studying the meridional circulation if care is taken in noting that the vertical diffusion of momentum has a substantial physical impact on the circulation (Adam, 2018; Adam & Harnik, 2013; Sobel & Schneider, 2009; Walker & Schneider, 2005). Some damping is necessary for any numerical model, but we have shown here that the values typically used in axisymmetric studies are large enough to mimic the impact of eddies on the circulation. Adam and Harnik (2013) demonstrate that parameterizing eddy momentum stresses, either implicitly through viscosity or explicitly, is one strategy for

exploring the parameter space of eddy impacts on the circulation. It can also ensure the proper scaling of the meridional and zonal circulation over a wide range of climates (Adam & Paldor, 2010; Walker & Schneider, 2006).

6. Conclusions

Our primary conclusions are the following:

1. In the presence of surface drag, a Hadley cell in an atmosphere with no resolved or parameterized eddy stresses cannot reach the surface.
   (a) With weak internal stresses, but sufficiently strong convection, the Hadley cell is unlikely to reach the surface.
2. It is possible to reproduce a nonaxisymmetric climate by applying time-mean eddy tendencies to an axisymmetric climate.

Regarding the latter, the time-mean eddy forcings on the atmosphere were explicitly calculated from an eddy-permitting simulation and applied to an axisymmetric simulation to characterize eddy impacts on the zonal-mean climate. Reproducing the zonal-mean climate required the consideration of eddy forcings on all prognostic variables, including processes other than internal atmospheric eddy fluxes such as surface fluxes and large-scale condensation. Neglecting these forcings results in substantial errors. Examination of vertically integrated heat and momentum budgets showed that the zonal-mean climate of the eddy-permitting simulation is well simulated by the axisymmetric simulation with all eddy forcings applied.

It is our hope that the technique presented here will be useful for understanding the response of any eddy-mean flow dynamic to various forcings. For example, one could apply the same climate forcing to both the eddy-permitting simulation and the axisymmetric simulation with all eddy forcings applied, such as a doubling of the longwave optical depth to simulate an increase in greenhouse gas concentrations. Examining the response of the eddy-permitting simulation will reveal the canonical greenhouse gas response, while examining the response of the axisymmetric simulation with all eddy forcings applied (and fixed to their unperturbed state) will reveal the direct mean flow response alone. Comparison of these two responses can provide insight into the role of eddies in driving circulation changes and changes in the broader climate. One could also apply the eddy forcings from the eddy-permitting simulation with a doubled optical depth to the unperturbed axisymmetric simulation (without doubling the optical depth). This would provide insight into the contribution of the perturbed eddies at equilibrium (as in this case, they are from a simulation where the eddies and mean flow have both adjusted to the forcing). The authors have already begun analyzing the results of such experiments. This technique could easily be generalized to stratosphere-troposphere coupling, future changes in the stratospheric residual circulation, and midlatitude eddy-driven jet variability, and can also be extended to more idealized momentum and heat forcings.

As a final caveat, some caution should be exercised as to how the results from this technique are interpreted. In particular, we have shown that we cannot perfectly recover the zonal-mean climate by applying the effects of the eddies to an axisymmetric simulation, even when we consider eddy impacts on surface fluxes and on convection. However, the imperfections in the technique are relatively small compared to the magnitude of typical climate forcings and the profound impact of the eddies on the circulation.

Appendix A: Eddy Terms in the Surface Pressure Tendency Equation

The surface pressure tendency equation is given by

$$\frac{\partial [p_s]}{\partial t} = -\int_0^{p_s} \nabla \cdot [v][p] \mathrm{d}p - \int_0^{p_s} \nabla \cdot [v'p'] \mathrm{d}p \tag{A1}$$

For a hybrid-sigma vertical coordinate system, the integral over layer k from pressure $p_{k-1/2}$ to $p_{k+1/2}$ can be expanded and discretized as

$$\int_{p_{k-1/2}}^{p_{k+1/2}} \nabla \cdot [\vec{v}'p'] \mathrm{d}p = \frac{\mathrm{d}b(k)}{a\cos(\phi)} \frac{\partial}{\partial \phi} \left[v'p'_s \cos(\phi) \right] \tag{A2}$$

where $\delta b(k)$ is the full-level sigma thickness given by $\delta b(k) = b(k + 1/2) - b(k - 1/2)$, where b are the sigma-level coefficients.

Acronyms

GRAM gray radiation aquaplanet model
NASA National Aeronautics and Space Administration
MERRA Modern-Era Retrospective ReAnalysis

Acknowledgments
The authors thank two anonymous reviewers for their insightful comments and suggestions. We also thank NASA's Global Modeling and Assimilation Office for creating and maintaining the MERRA2 reanalysis. MERRA2 was downloaded from NASA's GES Data and Information Services Center (https://gmao.gsfc.nasa.gov/reanalysis/MERRA-2/). Source code and sample scripts for GRAM are hosted by GFDL and available for download (https://www.gfdl.noaa.gov/idealized-moist-spectral-atmospheric-model-quickstart/). The modified source code is provided at https://github.com/nicholasadavis/gfdl_aquaplanet. Model output and basic technical support for the modifications is available from the corresponding author upon request. This work was partially supported by the U.S. National Science Foundation's Climate Dynamics Program (grant 1643167).

References

Adam, O. (2018). Zonally varying ITCZs in a Matsuno-Gill-type model with an idealized Bjerknes feedback. *Journal of Advances in Modeling Earth Systems*, *10*, 1304–1318. https://doi.org/10.1029/2017MS001183

Adam, O., & Harnik, N. (2013). Idealized annually averaged macroturbulent Hadley circulation in a shallow-water model. *Journal of the Atmospheric Sciences*, *70*, 284–302. https://doi.org/10.1175/JAS-D-12-072.1

Adam, O., & Paldor, N. (2010). On the role of viscosity in ideal Hadley circulation models. *Geophysical Research Letters*, *37*, L16801. https://doi.org/10.1029/2010GL043745

Adam, O., Schneider, T., & Harnik, N. (2014). Role of changes in mean temperatures versus temperature gradients in the recent widening of the Hadley circulation. *Journal of Climate*, *27*, 7450–7461. https://doi.org/10.1175/JCLI-D-14-00140.1

Andrews, D. G., Leovy, C., & Holton, J. (1987). *Middle atmosphere dynamics* (pp. 120–134). San Diego California: Academic Press.

Becker, E., Schmitz, G., & Gepr, R. (1997). The feedback of midlatitude waves onto the Hadley cell in a simple general circulation model. *Tellus A*, *49*, 182–199. https://doi.org/10.1034/j.1600-0870.1997.t01-1-00003.x

Birner, T., Davis, S. M., & Seidel, D. J. (2014). The changing width of Earth's tropical belt. *Physics Today*, *67*, 38–44. https://doi.org/10.1063/PT.3.2620

Bordoni, S., & Schneider, T. (2010). Regime transitions of steady and time-dependent Hadley circulations: Comparison of axisymmetric and eddy-permitting simulations. *Journal of the Atmospheric Sciences*, *67*, 1643–1654. https://doi.org/10.1175/2009JAS3294.1

Caballero, R. (2007). Role of eddies in the interannual variability of Hadley cell strength. *Geophysical Research Letters*, *34*, L22705. https://doi.org/10.1029/2007GL030971

Ceppi, P., & Hartmann, D. L. (2013). On the speed of the eddy-driven jet and the width of the Hadley cell in the Southern Hemisphere. *Journal of Climate*, *26*, 3450–3465. https://doi.org/10.1175/JCLI-D-12-00414.1

Davis, N. A., Seidel, D. J., Birner, T., Davis, S. M., & Tilmes, S. (2016). Changes in the width of the tropical belt due to simple radiative forcing changes in the GeoMIP simulations. *Atmospheric Chemistry and Physics*, *16*, 10,083–10,095. https://doi.org/10.5194/acp-16-10083-2016

DeCaria, A. J. (2006). Relating static energy to potential temperature: A caution. *Journal of the Atmospheric Sciences*, *64*, 1410–1412. https://doi.org/10.1175/JAS3906.1

Edmon, H. J., Hoskins, B. J., & McIntyre, M. E. (1980). Eliassen-Palm cross sections for the troposphere. *Journal of the Atmospheric Sciences*, *37*, 2600–2616. https://doi.org/10.1175/1520-0469(1980)037<2600:EPCSFT>2.0.CO;2

Fang, M., & Tung, K. K. (1999). Time-dependent nonlinear Hadley circulation. *Journal of the Atmospheric Sciences*, *56*, 1797–1807. https://doi.org/10.1175/1520-0469(1999)056<1797:TDNHC>2.0.CO;2

Frierson, D. M. W. (2007). The dynamics of idealized convection schemes and their effect of the zonally-averaged tropical circulation. *Journal of the Atmospheric Sciences*, *64*, 1959–1976. https://doi.org/10.1175/JAS3935.1

Frierson, D. M. W, Held, I. M., & Zurita-Gotor, P. (2006). A gray-radiation aquaplanet moist GCM. Part I: Static stability and eddy scales. *Journal of the Atmospheric Sciences*, *63*, 2548–2566. https://doi.org/10.1175/JAS3753.1

Frierson, D. M. W., Held, I. M., & Zurita-Gotor, P. (2007). A gray-radiation aquaplanet moist GCM. Part II: Energy transports in altered climates. *Journal of the Atmospheric Sciences*, *64*, 1680–1693. https://doi.org/10.1175/JAS3913.1

Frierson, D. M. W., Lu, J., & Chen, G. (2007). Width of the Hadley cell in simple and comprehensive general circulation models. *Geophysical Research Letters*, *34*, L18804. https://doi.org/10.1029/2007GL031115

Gelaro, R., McCarty, W., Suárez, M. J., Todling, R., Molod, A., Takacs, L., et al. (2017). The Modern-Era Retrospective Analysis for Research and Applications, Version 2 (MERRA-2). *Journal of Climate*, *30*, 5419–5454. https://doi.org/10.1175/JCLI-D-16-0758.1

Grise, K. M., & Polvani, L. M. (2016). Is climate sensitivity related to dynamical sensitivity? *Journal of Geophysical Research: Atmospheres*, *121*, 5159–5176. https://doi.org/10.1002/2015JD024687

Held, I. M. (2000). The general circulation of the atmosphere, Presented at the 2000 Woods Hole Oceanographic Institute Geophysical Fluid Dynamics Program, Woods Hole Oceanogr. Inst, Woods Hole, Mass. Available at http://gfd.whoi.edu/proceedings/2000/PDFvol2000.html

Held, I. M., & Hou, A. Y. (1980). Nonlinear axially symmetric circulations in a nearly inviscid atmosphere. *Journal of the Atmospheric Sciences*, *37*, 515–533. https://doi.org/10.1175/1520-0469(1980)037<0515:NASCIA>2.0.CO;2

Hu, Y., Tao, L., & Liu, J. (2013). Poleward expansion of the Hadley circulation in CMIP5 simulations. *Advances in Atmospheric Sciences*, *30*, 790–795.

Jucker, M., & Gerber, E. P. (2017). Untangling the annual cycle of the tropical tropopause layer with an idealized moist model. *Journal of Climate*, *30*, 7339–7358. https://doi.org/10.1175/JCLI-D-17-0127.1

Kim, H.-K., & Lee, S. (2001). Hadley cell dynamics in a primitive equation model. Part II: Nonaxisymmetric flow. *Journal of the Atmospheric Sciences*, *10*, 2859–2871. https://doi.org/10.1175/1520-0469(2001)058<2859:HCDIAP>2.0.CO;2

Klinger, B. A., & Marotzke, J. (2000). Meridional heat transport by the subtropical cell. *Journal of Physical Oceanography*, *30*, 696–705. https://doi.org/10.1175/1520-0485(2000)030<0696:MHTBTS>2.0.CO;2

Korty, R. L., & Schneider, T. (2008). Extent of Hadley circulations in dry atmospheres. *Geophysical Research Letters*, *35*, L23803. https://doi.org/10.1029/2008GL035847

Kushner, P. J., & Polvani, L. M. (2004). Stratosphere–troposphere coupling in a relatively simple AGCM: The role of eddies. *Journal of Climate*, *17*, 629–639. https://doi.org/10.1175/1520-0442(2004)017<0629:SCIARS>2.0.CO;2

Levine, X. J., & Schneider, T. (2011). Response of the Hadley circulation to climate change in an aquaplanet GCM coupled to a simple representation of ocean heat transport. *Journal of the Atmospheric Sciences*, *68*, 769–783. https://doi.org/10.1175/2010JAS3553.1

Levine, X. J., & Schneider, T. (2015). Baroclinic eddies and the extent of the Hadley circulation: An idealized GCM study. *Journal of the Atmospheric Sciences*, *72*, 2744–2761. https://doi.org/10.1175/JAS-D-14-0152.1

Lindzen, R. S., & Hou, A. Y. (1988). Hadley circulations for zonally averaged heating centered off the equator. *Journal of the Atmospheric Sciences*, *45*, 2416–2427. https://doi.org/10.1175/1520-0469(1988)045<2416:HCFZAH>2.0.CO;2

Lu, J., Vecchi, G. A., & Reichler, T. (2007). Expansion of the Hadley cell under global warming. *Geophysical Research Letters*, *34*, L06805. https://doi.org/10.1029/2006GL028443, https://doi.org/10.1007/200376-012-2187-4

Pauluis, O., Czaja, A., & Korty, R. (2008). The global atmospheric circulation on moist isentropes. *Science*, *321*, 1075–1078. https://doi.org/10.1126/science.1159649

Schneider, T., & Bordoni, S. (2008). Eddy-mediated regime transitions in the seasonal cycle of a Hadley circulation and implications for monsoon dynamics. *Journal of the Atmospheric Sciences*, *65*, 915–933. https://doi.org/10.1175/2007JAS2415.1

Seidel, D. J., Fu, Q., Randel, W. J., & Reichler, T. J. (2008). Widening of the tropical belt in a changing climate. *Nature Geoscience*, *1*, 21–24. https://dx.doi.org/10.1038/ngeo.2007.38

Sobel, A. H., & Schneider, T. (2009). Single-layer axisymmetric model for a Hadley circulation with parameterized eddy momentum forcing. *Journal of Advances in Modeling Earth Systems*, *1*, 10. https://doi.org/10.3894/JAMES.2009.1.10

Stone, P. H., Quirk, W. J., & Somerville, R. C. (1974). The effect of small-scale vertical mixing of horizontal momentum in a general circulation model. *Monthly Weather Review*, *102*, 765–771. https://doi.org/10.1175/1520-0493(1974)102<0765:TEOSSV>2.0.CO;2

Trenberth, K. E., & Stepaniak D. P. (2003). Seamless poleward atmospheric energy transports and implications for the Hadley circulation. *Journal of Climate*, *16*, 3706–3722. https://doi.org/10.1175/1520-0442(2003)016<3706:SPAETA>2.0.CO;2

Walker, C. C., & Schneider, T. (2005). Response of idealized Hadley circulations to seasonally varying heating. *Geophysical Research Letters*, *32*, L06813. https://doi.org/10.1029/2004GL022304

Walker, C. C., & Schneider, T. (2006). Eddy influences on Hadley circulations: Simulations with an idealized GCM. *Journal of the Atmospheric Sciences*, *63*, 3333–3350. https://doi.org/10.1175/JAS3821.1

Waugh, D., Grise, K. M., Seviour, W. J., Davis, S., Davis, N., Adam, O., et al. (2018). Revisiting the relationship among metrics of tropical expansion. *Journal of Climate*, *31*, 7565–7581. https://doi.org/10.1175/JCLI-D-18-0108.1

Williams, G. P. (2003). Jet sets. *Journal of the Meteorological Society of Japan*, *81*, 439–476. https://doi.org/10.2151/jmsj.81.439

Wirth, V., & Dunkerton, T. J. (2006). A unified perspective on the dynamics of axisymmetric hurricanes and monsoons. *Journal of the Atmospheric Sciences*, *63*, 2529–2547. https://doi.org/10.1175/JAS3763.1

Zurita-Gotor, P., & Álvarez-Zapatero, P. (2018). Coupled interannual variability of the Hadley and Ferrel cells. *Journal of Climate*, *31*, 4757–4773. https://doi.org/10.1175/JCLI-D-17-0752.1